# Asymmetric oscillations of endoskeletal antibubbles

Nobuki Kudo, Rustem Uzbekov, Ryunosuke Matsumoto, Ri-Ichiro Shimizu, Craig Stuart Carlson, Nicole Anderton, Aurélie Deroubaix, Clement Penny, Albert Thijs Poortinga, David Milton Rubin, et al.

# Asymmetric oscillations of endoskeletal antibubbles

Nobuki Kudo[1]*, Rustem Uzbekov[2,3], Ryonosuke Matsumoto[1], Ri-ichiro Shimizu[1], Craig S. Carlson[4], Nicole Anderton[4], Aurélie Deroubaix[5], Clement Penny[5], Albert T. Poortinga[6], David M. Rubin[4], Ayache Bouakaz[7], and Michiel Postema[4]

[1]*Faculty of Information Science and Technology, Hokkaido University, Kita 14 Chome, Nishi 9 Jo, Kita-ku, Sapporo, Hokkaido 060-0814, Japan*

[2]*Department of Microscopy, Faculty of Medicine, University of Tours, 10 Boulevard Tonnellé, 37000 Tours, France*

[3]*Faculty of Bioengineering and Bioinformatics, Moscow State University, ul. Leninskiye Gory 1/73, Moscow 119192, Russia*

[4]*School of Electrical and Information Engineering, University of the Witwatersrand, Johannesburg, 1 Jan Smuts Laan, 2001 Braamfontein, South Africa*

[5]*Department of Internal Medicine, University of the Witwatersrand, Johannesburg, 7 York Road, 2193 Parktown, South Africa*

[6]*Department of Mechanical Engineering, Eindhoven University of Technology, De Zaale, 5600 MB Eindhoven, Netherlands*

[7]*Inserm U1253, Faculty of Medicine, University of Tours, 10 Boulevard Tonnellé, 37000 Tours, France*

Antibubbles have been under investigation as potential vehicles in ultrasound-guided drug delivery. It is assumed that antibubbles can expand unhampered, but cannot contract beyond the size of their inner core. In this study, this hypothesis was tested on endoskeletal antibubbles and reference bubbles. These were subjected to 3-cycle pulses of 1-MHz ultrasound, whilst being recorded with a high-speed camera operating at 10 million frames per second. At low acoustic amplitudes (200 kPa), antibubbles and bubbles oscillated symmetrically. At high acoustic amplitudes (1.00 MPa), antibubbles and bubbles oscillated asymmetrically, but antibubbles significantly more so than bubbles. Furthermore, fragmentation and core release were observed at these amplitudes. This finding may have implications for ultrasound-guided drug delivery using antibubbles.

Ultrasound contrast agents comprise suspensions of micrometer-sized gas bubbles, each surrounded by a stabilising shell.[1)] In ultrasound fields, these so-called microbubbles oscillate, *i.e.*, they subsequently expand and contract, creating a secondary sound field that can be detected with imaging equipment. Consequently, injections of ultrasound contrast agents have been utilised for diagnostic medical imaging.[2–4)] Oscillating microbubbles may interact with living cells and tissue.[5–7)] Therefore, ultrasound contrast agents have also, more recently, been

*E-mail: kudo@ist.hokudai.ac.jp

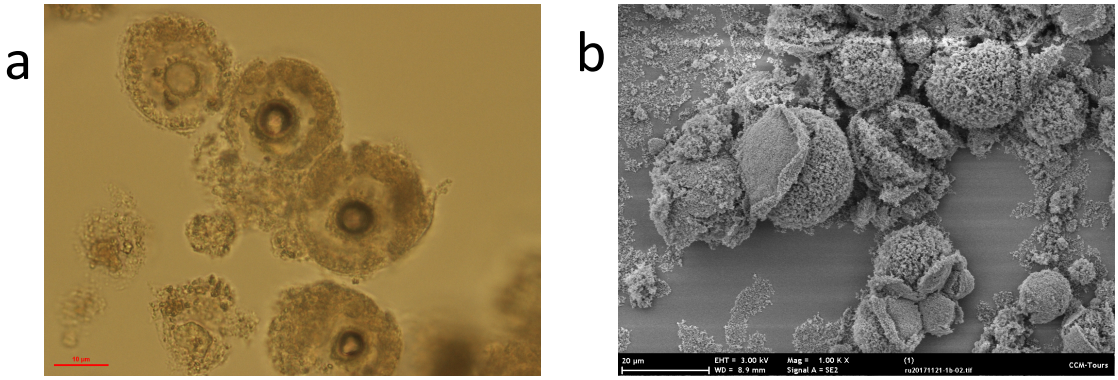


**Fig. 1.** Brightfield microscopic image of four endoskeletal antibubbles, with approximate inner droplet diameters of 5 $\mu$m (a). The scaling bar corresponds to 10 $\mu$m. Scanning electron microscope image of an endoskeletal antibubble (b). Ruptured silica membranes reveal skeletal structures underneath. The scaling bar corresponds to 20 $\mu$m. This image is a zoomed-out version of Fig. 1 in Ref. 21.

introduced in therapeutic settings.[8–10] One of the most popular ways to study microbubbles subjected to ultrasound is with high-speed photography.[11–14]

Antibubbles are gas bubbles in suspension containing a liquid core droplet. Antibubbles with surfactant interfaces are short-lived, with drainage times within 1000 seconds.[15,16] By adding nanoparticles to the interfaces, antibubbles can be produced with long lifespans.[17,18] Antibubbles have been produced with microfluidics, too.[19] Please note that these droplets are suspending inside the bubbles owing to electrostatic forces. By adding a hydrophobic endoskeleton, the droplets can be fixed in position inside the bubble. Endoskeletal antibubbles have been recently demonstrated.[21] This study follows up by showing full results of endoskeletal antibubble dynamics.

Figure 1a shows a brightfield microscopic image of endoskeletal antibubbles in EPON resin. The top halves of the bubbles had been cut off with a diamond knife without violating the integrity of the antibubbles. Four antibubbles contain a single droplet core of approximately 5-$\mu$m diameter. The endoskelotons themselves are shown in Figure 1b. The silica particles on the outer interface have been reported to form a single elastic layer.[22] The same batch of the antibubbles used to create Figure 1 has been used for the experiments described in this paper.

Shortly after the first high-speed camera observation of ultrasonic antibubbles, they were proposed as a vehicle to carry drugs to a region of interest, to be released using clinical ultrasound.[20] Antibubbles have proven to be suitable ultrasound contrast agents for harmonic imaging, as well.[22] The unique harmonic features of antibubbles have been attributed to the assumption that antibubbles can expand unhampered, but cannot contract beyond the size of their inner core.[23] In a simulation study, the outward expansion was shown to surpass that

of bubbles without a core droplet, whilst the contraction of antibubbles is less than that of bubbles without core droplets.[24)]

Antibubbles have a higher resonance frequency than their bubble counterparts.[25)] By modifying eq. (2.2.7) in Ref. 25 to contain the entire volumetric incompressible content $V_\mathrm{i}$ and ignoring the presence of an outer elastic shell, the linear resonance frequency $f_\mathrm{r}$ of the endoskeletal antibubble becomes:

$$f_\mathrm{r} = \frac{1}{2\pi R_0\sqrt{\rho}}\sqrt{\frac{3\gamma\left(p_0 - p_\mathrm{v} + \frac{2\sigma}{R_0}\right)}{1 - \frac{3V_\mathrm{i}}{4\pi R_0^3}} - \frac{2\sigma}{R_0} - \frac{4\eta^2}{R_0^2\rho}}, \tag{1}$$

where $p_0$ is the ambient pressure, $p_\mathrm{v}$ is the vapour pressure, $R_0$ is the equilibrium bubble radius, $\gamma$ is the polytropic exponent of the gas, $\eta$ is the liquid viscosity, $\rho$ is the liquid density, and $\sigma$ is the surface tension. Obviously, $0 \leq V_\mathrm{i} < \frac{4}{3}\pi R_0^3$. Thus, the presence of an endoskeleton increases the resonance frequency even more.

Two media containing (anti)bubbles were prepared for evaluation, as previously published.[18,22)] For stabilisation, Aerosil® R972 hydrophobised silica particles (Evonik Industries AG, Essen, Germany) were used.[22)]

For the first medium, hereafter referred to as AB, the aqueous cores were replaced by 2 vol% of hydrophobically modified Zano 10 Plus zinc oxide nanoparticles (Umicore, Brussel, Belgium). Instead of the formation of just droplets inside antibubbles, adding nanoparticles creates an endoskeletal structure with one or multiple voids that can be liquid-filled.[17,18,21)]

The second medium was left without cores, so it contained stabilised bubbles instead of antibubbles. This medium served as reference medium, hereafter referred to as REF.

For each medium, 5 mg of freeze-dried material was deposited into a FALCON® 15 mL High-Clarity Polypropylene Conical Tube (Corning Science México S.A. de C.V., Reynosa, Tamaulipas, Mexico), after which 5 mL of 049-16797 Distilled Water (FUJIFILM Wako Pure Chemical Corporation, Chuo-Ku, Osaka, Japan) was added.

Each emulsion was gently shaken by hand for 1 minute, after which 200 $\mu$L was pipetted into the observation chamber of a high-speed observation system.[26)] The observation chamber was placed under an Eclipse Ti inverted microscope (Nikon Corporation, Minato-ku, Tokyo, Japan) with a Plan Apo LWD 40× WI (N.A. 0.8) objective lens. Attached to the microscope was an HPV-X2 high-speed camera (Shimadzu, Nakagyo-ku, Kyoto, Japan), operating at 10 million frames per second.[27)]

During camera recording, the materials were subjected to ultrasound pulses, each comprising 3 cycles with a centre transmitting frequency of 1.00 MHz and a peak-negative pressure

of 200 kPa (1 V input) or 1.00 MPa (5 V input), from a laboratory-assembled single-element transducer.[26,27)]

The transducer was driven by a signal generated by an AFG320 arbitrary function generator (Sony-Tektronix, Shinagawa-ku, Tokyo, Japan) and amplified by a UOD-WB-1000 wide-band power amplifier (TOKIN Corporation, Shiroishi, Miyagi, Japan).

The videos recorded were segmented and analysed using MATLAB® (The MathWorks, Inc., Natick, MA, USA). In the first frame of each video, objects in the field of view were identified. These were then automatically sized throughout the rest of the video, resulting in radius(time) curves. For each radius(time) curve, the equilibrium radius, $R_0$, the maximum radius during the first cycle, $R_{\max}$, and the first minimum radius after the transient phase, $R_{\min}$, were determined. From these, positive excursion, $\xi^+ = (R_{\max} - R_0)$, and negative excursion, $\xi^- = (-R_{\min} + R_0)$, were determined, yielding the absolute oscillation asymmetry $(\xi^+ - \xi^-) = (R_{\max} + R_{\min} - 2R_0)$. Although $(\xi^+ - \xi^-) = (R_{\max} + R_{\min} - 2R_0)$ is a direct quantifyer of asymmetry, it must be noted that the values measured are greatly influenced by the accuracy of determining $R_0$.

Brightfield microscope $z$-stack galleries were captured using the brightfield component of a ZEISS LSM 780 confocal laser scanning microscope with an alpha Plan-Apochromat 63×/1.40 NA Oil CorrM27 objective lens (Carl Zeiss AG, Oberkochen, Germany).

Figure 2 shows a $z$-stack of brightfield microscopy images of an endoskeletal antibubble. In the focal plane (middle frame) and the planes right above and below focus, droplets of diameters less than 1 $\mu$m can be observed, indicated by dark spots, as well as entrapped gas cavities, indicated by white spots. In brightfield microscopy, denser regions appear darker, whilst less dense regions appear brighter.[28)] The space between the hydrophobised zinc oxide endoskeleton and the hydrophobised silica membrane is a gaseous void, shown as a white ring in frames 4–6.

Figure 3 shows the equilibrium radius $R_0$ versus the maximum expansion $R_{\max}$ and contraction $R_{\min}$ measured from a total of thirty-three high-speed videos with 118 AB and 144 REF, for acoustic pressure amplitudes of 200 kPa and 1.00 MPa. At 200-kPa acoustic amplitude, REF has slightly higher excursions than AB. At 1.00-MPa amplitude, AB has substantially greater expansion ($R_{\max} = 1.5R_0 + 1.5\ \mu$m), whereas REF has greater contraction ($R_{\min} = 0.57R_0 + 0.07\ \mu$m).

l This is even more evident from the difference in least-squares solutions. At 200-kPa amplitude, for both AB and REF, $(\xi^+ - \xi^-) \approx 0$, *i.e.*, both oscillate symmetrically despite occasional asymmetry. However, at 1.00-MPa amplitude, for AB: $(\xi^+ - \xi^-) = 0.30R_0 +$

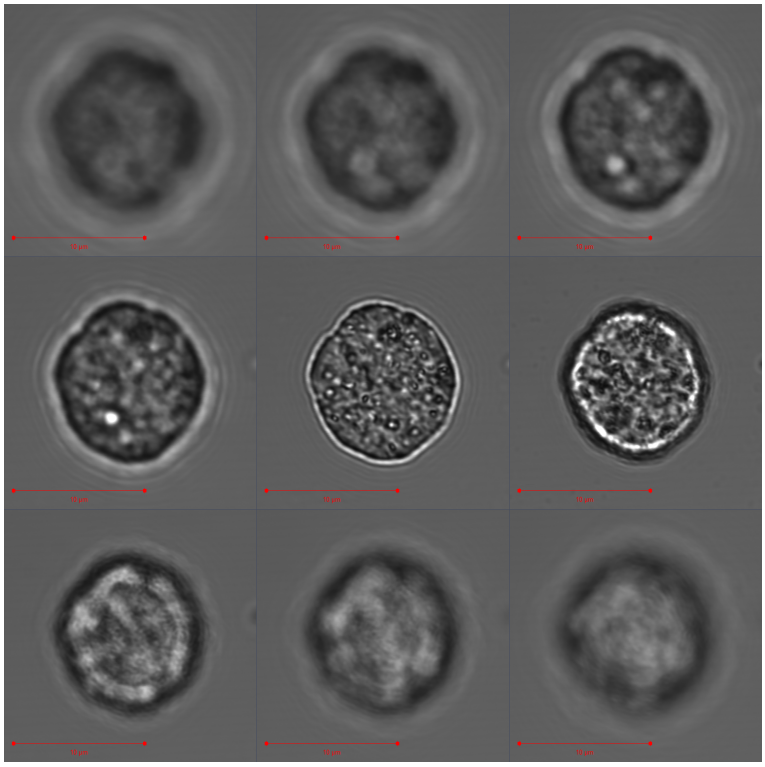

**Fig. 2.** Brightfield microscopy $z$-stack gallery of AB, captured over a 24-$\mu$m range at 3-$\mu$m intervals. The scaling bars correspond to 10 $\mu$m. Frames run from left–right, top–bottom.

1.2 $\mu$m, whereas for REF, $(\xi^+ - \xi^-) = 0.20R_0 + 1.5\,\mu$m. Thus, although both AB and REF oscillate asymmetrically, AB oscillates significantly more asymmetrically than REF.

It must be noted that the resonance frequency of these endoskeletal antibubbles must be substantially greater than 1 MHz.[23] Consequently, treating the maximum and minimum expansion as a linear case is justified.

Interestingly, in the same high-amplitude regime, the antibubbles can be observed to release their core contents. Figure 4 shows 4 frames selected from 256 frames of a high-speed video with AB sonicated at a 1.00-MPa amplitude. After the first oscillation cycle, the surface instabilities leading to fragmentation can be clearly seen. After sonication, the antibubble fragments were scattered around the remains of a bubble. This bubble remained acoustically active during subsequent pulses (not shown).

While low-amplitude pulses did not change the contents of the antibubble,[21] a short high-amplitude pulse could disrupt antibubbles within three cycles.

The high-speed videos confirm the expansion-only hypothesis at 1-MPa acoustic amplitude at a transmitting frequency of 1 MHz.

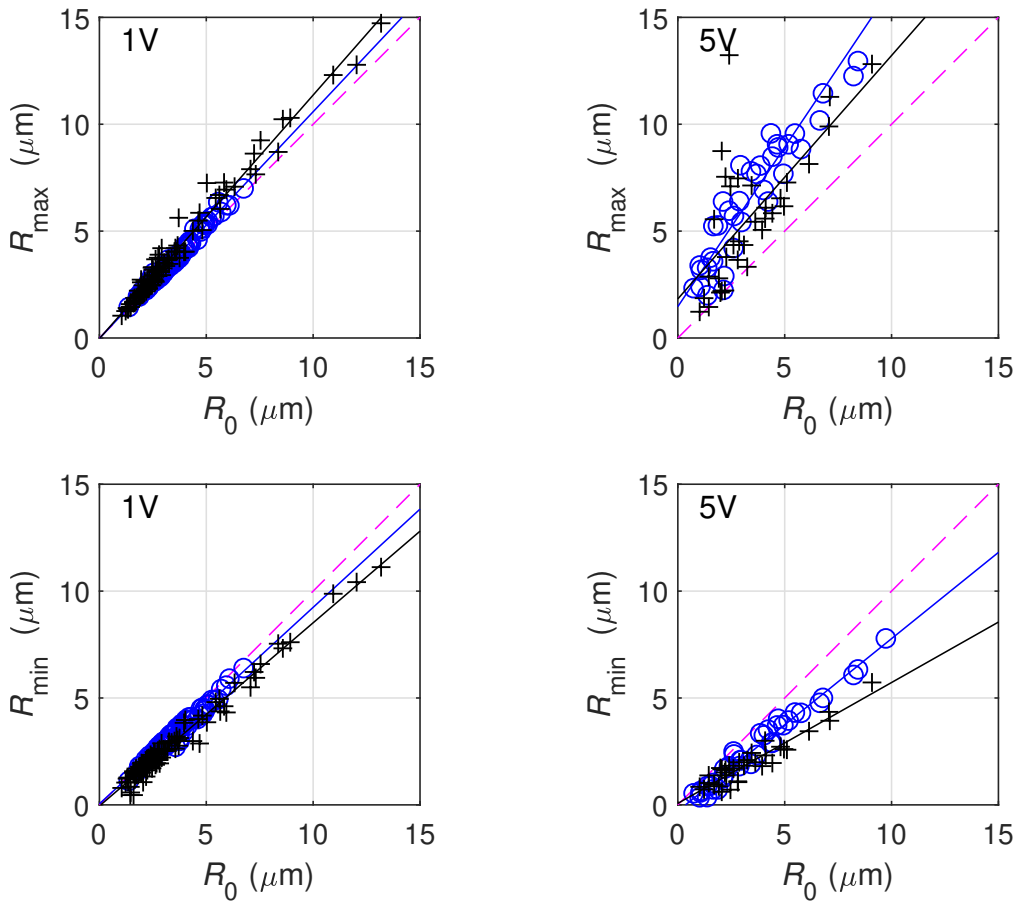


**Fig. 3.** Equilibrium radius $R_0$ versus maximum expansion $R_{max}$ (top) and contraction $R_{min}$ (bottom), for acoustic pressure amplitudes of 200 kPa (1V, left) and 1.00 MPa (5V, right). The dashed purple lines correspond to $R_{m*} = R_0$, the blue and black lines represent the least-squares solutions for AB (o) and REF (+), respectively.

One short, high-amplitude pulse appeared to be enough to shatter antibubbles and release their core contents. This finding may have implications for ultrasound-guided drug delivery using antibubbles.

**Acknowledgements** The scanning electron microscope data were obtained with the aid of the IBiSA Electron Microscopy Facility of the University of Tours and the University Hospital of Tours. Laser scanning confocal microscopy was performed at the Life Sciences Imaging Facility of the University of the Witwatersrand, Johannesburg. This work has been supported by JSPS KAKENHI Grant Number 17H00864.

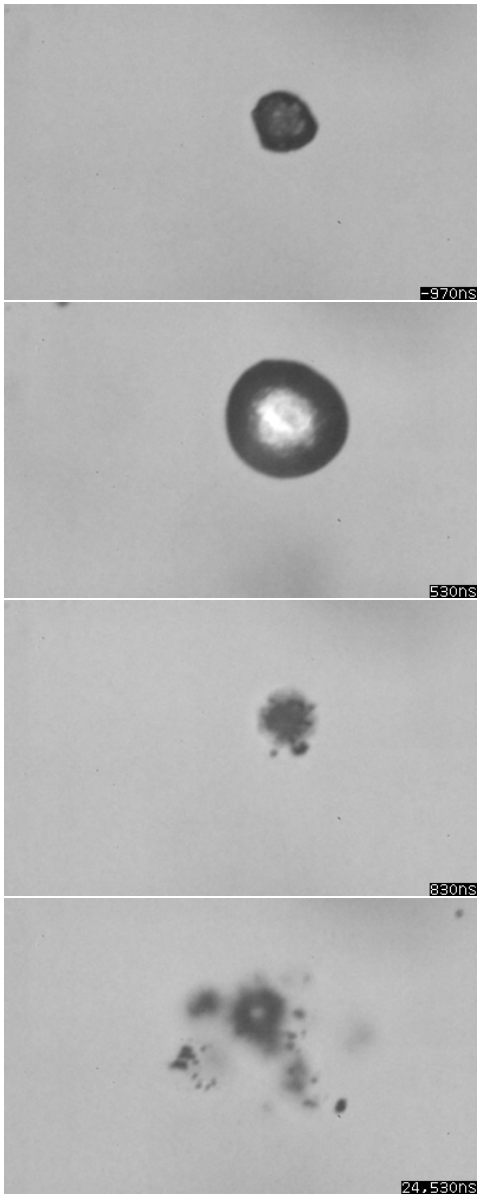


**Fig. 4.** Four high-speed frames of sonicated AB. Top-bottom: before sonication; during the first rarefactional peak; fragmentation during contraction; after sonication. Each frame width corresponds to 145 $\mu$m. Time stamps relative to ultrasound arrival indicate −970 ns, 530 ns, 830 ns, and 24,530 ns.

## References


1) V. Paefchen, D. Doleschel, and F. Kiessling, Front. Pharmacol. **6** 197 (2015).
2) S. Ishikura, M. Yoshizawa, N. Tagawa, and T. Irie, Jpn. J. Appl. Phys. **57** 07LF20 (2018).
3) R. R. Wildeboer, R. J. G. van Sloun, P. Huang, H. Wijkstra, and M. Mischi, Ultrasound Med. Biol. **45** 2713 (2019).
4) J. Quan, Y. Hong, X. Zhang, M. Mei, X. You, and P. Huang, Clin. Hemorheol. Microcirc. **72** 293 (2019).
5) R. Oitate, A. Shimomura, H. Wada, T. Mochizuki, K. Masuda, Y. Oda, R. Suzuki, and K. Maruyama, Jpn. J. Appl. Phys. **56** 07JF25 (2017).
6) R. Oitate, T. Otsuka, M. Seki, A. Furutani, T. Mochizuki, K. Masuda, R. Suzuki, and K. Murayama, Jpn. J. Appl. Phys. **57** 07LF10 (2018).
7) T. Sato and K. Ikeda, Jpn. J. Appl. Phys. **57** 07LF16 (2018).
8) S. Kotopoulis, G. Dimcevski, O. H. Gilja, D. Hoem, and M. Postema, Med. Phys. **40** 072902 (2013).
9) R. H. Rahayu, K. Takanashi, T. T. K. Soon, I. Seviaryna, R. Maev, K. Kobayashi, N. Hozumi, and S. Yoshida, Jpn. J. Appl. Phys. **56** 07LF26 (2017).
10) Wang G, Li Q, Chen D, Wu B, Wu Y, Tong W, and Huang P. Theranostics **9** 6191 (2019).
11) M. Postema, A. van Wamel, F. J. ten Cate, and N. de Jong, Med. Phys. **32** 3707 (2005).
12) K. Suzuki, R. Iwasaki, R. Takagi, S. Yoshizawa, and S. Umemura, Jpn. J. Appl. Phys. **56** 07JF27 (2017).
13) N. Okada, M. Shiiba, S. Yamauchi, T. Sato, and S. Takeuchi, Jpn. J. Appl. Phys. **57** 07LE15 (2018).
14) S. Nishitaka, D. Mashiko, S. Yoshizawa, and S. Umemura, Jpn. J. Appl. Phys. **57** 07LF25 (2018).
15) B. Scheid, S. Dorbolo, L. R. Arriaga, and E. Rio, Phys. Rev. Lett. **109** 264502 (2012).
16) Y. Vitry, S. Dorbolo, J. Vermant, and B. Scheid, Adv. Colloid Interface Sci. **270** 73 (2019).
17) A. T. Poortinga, Langmuir **27** 2138 (2011).
18) A. T. Poortinga, Colloid. Surf. A: Physicochem. Eng. Aspects **419** 15 (2013).
19) J. E. Silpe, J. K. Nunes, A. T. Poortinga, and H. A. Stone, Langmuir **29** 8782 (2013).
20) M. Postema, N. de Jong, G. Schmitz, and A. van Wamel, Proc. 2005 IEEE Ultrason. Symp. 977 (2005).
21) N. Kudo, R. Uzbekov, R. Matsumoto, R. Shimizu, C. Carlson, N. Anderton,

A. Deroubaix, C. Penny, A. T. Poortinga, D. M. Rubin, A. Bouakaz, and M. Postema, Proc. 40th Symp. UltraSon. Electron. 2E3-1 (2019).

22) M. Postema, A. Novell, C. Sennoga, A. T. Poortinga, and A. Bouakaz, Appl. Acoust. **137** 148 (2018).

23) K. Johansen and M. Postema, Hydroacoustics **19** 197 (2016).

24) K. Johansen, S. Kotopoulis, A. T. Poortinga, and M. Postema, Physics Procedia **70** 1079 (2015).

25) S. Kotopoulis, K. Johansen, O. H. Gilja, A. T. Poortinga, and M. Postema, Acta Phys. Polon. A **127** 99 (2015).

26) N. Kudo, IEEE Trans. Ultrason. Ferroelect. Freq. Control **64** 273 (2017).

27) S. Imai and N. Kudo, IEEE Int. Ultrason. Symp. **IUS2018** 184 (2018).

28) M. Postema, A. Bouakaz, C. T. Chin, and N. de Jong, IEEE Trans. Ultrason. Ferroelect. Freq. Control **50** 523 (2003).